Bianthrone in a Single-Molecule Junction: Conductance Switching with a Bistable Molecule Facilitated by Image Charge Effects†

ARTICLE *in* THE JOURNAL OF PHYSICAL CHEMISTRY C · OCTOBER 2010

Impact Factor: 4.77 · DOI: 10.1021/jp1060667

7 AUTHORS, INCLUDING:

Samuel Lara-Avila
Chalmers University of Technology
49 PUBLICATIONS **752** CITATIONS
SEE PROFILE

Andrey V Danilov
Chalmers University of Technology
36 PUBLICATIONS **967** CITATIONS
SEE PROFILE

Victor Geskin
Université de Mons
75 PUBLICATIONS **1,782** CITATIONS
SEE PROFILE

Jérôme Cornil
Université de Mons
291 PUBLICATIONS **15,584** CITATIONS
SEE PROFILE

Bianthrone in a Single-Molecule Junction: Conductance Switching with a Bistable Molecule Facilitated by Image Charge Effects†

Samuel Lara-Avila,‡ Andrey Danilov,‡ Victor Geskin,§ Saïd Bouzakraoui,§ Sergey Kubatkin,‡ Jérôme Cornil,*,§ and Thomas Bjørnholm||

Department of Microtechnology and Nanoscience, Chalmers University of Technology, Kemivägen 9, S-41296 Göteborg, Sweden, Service de Chimie des Matériaux Nouveaux, Université de Mons, Place du Parc 20, B-7000 Mons, Belgium, and Nano-Science Center & Department of Chemistry, University of Copenhagen, Universitetsparken 5, DK-2100 Copenhagen, Denmark

Received: July 1, 2010; Revised Manuscript Received: September 23, 2010

Bianthrone is a sterically hindered compound that exists in the form of two nonplanar isomers. Our experimental study of single-molecule junctions with bianthrone reveals persistent switching of electric conductance at low temperatures, which can be reasonably associated with molecular isomerization events. Temperature dependence of the switching rate allows for an estimate of the activation energy of the process, on the order of 120 ± 50 meV. Quantum-chemical calculations of the potential energy relief of neutral bianthrone and its anion, including identification of transition states, yields the isolated molecule isomerization barriers too high vs the previous estimate, though compatible with previous experimental studies in solution. Nevertheless, we show that the attraction of the anion in the vicinity of the metal surface by its image charge can change the energetic landscape, in particular, by significantly reducing the barrier to values compatible with the observed switching behavior.

Introduction

Molecular electronics is a fast developing field which has a potential to dramatically extend the miniaturization limits of the integrated circuit technology. The ultimate ambition of molecular electronics is to implement the desired electronic functionality at a single-molecule level by a proper molecular design.[1] Spectacular recent advances in experimental techniques made it possible to bridge a single molecule to macroscopic electrodes and to study current transport through a molecule in two- and three-terminal devices.[2] Molecular resonance tunneling devices,[3] single electron transistors,[4,5] and switches[6] were demonstrated.

In view of possible device applications, molecular switches appear to be the most promising candidates as CMOS successors. First of all, switches are the basic elements for digital memory and field programming gate arrays (FPGA) - the two large groups of electronic devices that will benefit the most from radical miniaturization to be provided by molecular implementation. Moreover, both memory chips and FPGAs are regular arrays of many identical units and the technology shall clearly benefit from the fact that chemical synthesis can provide moles of identical functional kernels.

Three different design concepts for molecular switches were suggested so far: (I) switches operating by reversible isomerization without pronounced changes in molecular shape like tautomerization,[7] opening/closing of conjugation path,[8] or intramolecular charge redistribution;[9] (II) switches exploiting rotation or rolling of the whole molecule;[10] (III) conformational switches based on isomerization between two manifestly different metastable shapes predetermined by molecular design (two states can differ, for example, by folding[11,12] or twisting[13,14] a part of the molecule around flexible link or by sliding[15] or circumrotation[16] of a molecular component in mechanically interlocked supramolecular structures).

The main challenge on the way to a wafer-scale fabrication lies in a poor reproducibility of single-molecule devices. Being identical in solution, molecular kernels reveal big dispersion of operational parameters when placed in a solid-state environment. For example, it is currently a well-established fact that molecular electronic spectrum and addition energies can be dramatically affected by image charges generated in the substrate and electrodes.[4,17,18] Small variations in molecular placement/orientation redistribute these image charges, which makes operational parameters of class I switches vulnerable to environmental effects and difficult to predict judging from the properties of functional molecules measured in solution. Class II switches suffer from high sensitivity of molecule-to-electrode coupling to intimate details of atomic arrangement within the contact area; a single atom displacement can, and often does dramatically affect the switching behavior.[10]

Conceptually, the conformational switches have a potential to be less prone to environmental uncertainties. In this paper, we present a conformational switch based on the bianthrone (BA) molecule, which has two well-defined conformations,[19] as illustrated in Figure 1. The structural constraint that ensures the existence of two forms cannot be overruled by any environmental perturbations as long as the molecule retains its chemical identity. One can therefore expect that the switching behavior will be a robust feature of bianthrone single molecule junctions. Indeed, we observed the hysteretic switching between two states with different conductancies in all measured samples. However, the data analysis shows that the environment does play an important role: the barrier which separates two conformations is dramatically reduced. We argue that this effect

† Part of the "Mark A. Ratner Festschrift".

* Corresponding author. E-mail: Jerome.Cornil@umons.ac.be.
‡ Chalmers University of Technology.
§ Université de Mons.
|| University of Copenhagen.

10.1021/jp1060667
Published on Web 10/19/2010

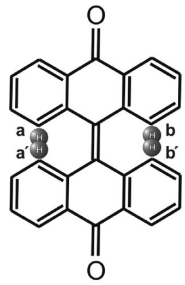

Figure 1. Valence structure and the origin of two conformations of bianthrone. In form A, protons **a′**, **b′** are on top and **a**, **b** beneath; in form B, **a**, **b′** are on top and **a′**, **b** beneath.

can be attributed to interaction between charges on the molecule and highly polarizable environment.

BA belongs to a family of overcrowded bistricyclic aromatic enes (BAEs).[20,21] A coplanar conformation of the molecule, though favorable for conjugation, is sterically impossible because of overcrowding in the vicinity of the double bond in the middle (in the "fjord" region): two hydrogen atoms (**a** and **a′** in Figure 1) cannot share the same space: either **a** or **a′** should be on top of the other. A similar constraint, of course, applies to the complementary pair **bb′.** Two distinct conformations (**A** and **B**) arise from two ways for the molecule to reduce the strain by out-of-plane deformation: (i) by sacrificing the planarity of the anthrones but conserving the coplanarity around the double bond in the folded conformation **A**, where two protons linked to the same anthrone group are both on top, (ii) by conserving the former and sacrificing the latter in the twisted conformation **B**, where one proton is on top and the other underneath.

Furthermore, there is a pronounced difference in the electronic properties of the isomers: the thermochromism of bianthrone discovered a century ago was successfully attributed to isomerization when the structure and energetics of both forms were uncovered.[19,22]

In neutral BA, the folded A-form is more stable, but the relative stability of the forms is reversed upon reduction, in favor of the twisted B-form, more stable in anions and dianions, as established electrochemically.[23,24] Electrochemical reduction of the A-form in solution is thus associated with isomerization to the B-form, while the oxidation leads to the isomerization back to the A-form as the molecule returns to the neutral state. Thus, reversible switching of BA between its isomers can be realized under electrochemical stimulus in the bulk.

An early attempt to make use of the inversed stability of the isomers in neutral and negative BA for a molecular switch[25,26] consisted of coupling BA to an electron acceptor to induce electron transfer to BA by photoexcitation. Unfortunately, the ordering of the excited states turned out to be unfavorable for photoinduced switching in this system.

In a similar context, an STM study[27] of monolayers of a substituted bianthrone on Cu(111) suggested that the molecules adopt their A-conformation and their chemisorption to the substrate was not strong enough to hinder conformational transitions. Moreover, in some cases they observed the molecule at the domain edges appearing asymmetric, thus probably adopting their B-conformation. The possibility to address each molecule individually with an STM tip places this setup closer to the single-molecule switch concept, though no deterministic switching was observed in this study.

In this work, we demonstrate experimentally that single-molecule BA junctions reveal two states with different conductance and hysteretic ON and OFF switching. We analyze the temperature dependence of the switching voltages at temperatures as low as 4−19 K and conclude that in a planar device the barrier that separates two conformations is dramatically reduced (down to ∼70−170 meV) as compared to that for BA in solution (∼1 eV). This apparent discrepancy motivated us to study theoretically the rearrangement of bianthrone, first, as an isolated molecule and then at the surface of a solid. The dramatic effect of a polarizable environment leading to decreased energy level spacing, as it manifests in electronic excitation spectra, is now widely recognized.[17,18] Here, we argue that similar renormalization can also occur for the barrier height due to the image charge effect following structural changes: the geometries of different isomers of the charged molecule and the transition state are responsive to their image charges, which leads to one moiety being effectively stabilized by interaction with the substrate via the image charge forces.

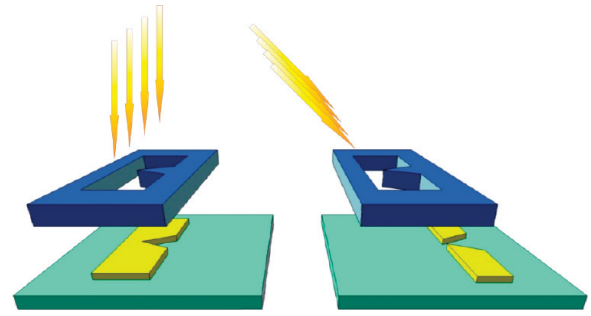

Figure 2. Tuning the nanogap width by deposition at an angle. Left: for normal deposition the result is a strip with constriction about 50 nm wide. Right: for deposition at a 45° angle the result is two leads separated with a gap ∼20 nm wide. At some critical angle $0 < \alpha_C < 45°$, the gap separating two leads will squeeze to zero. The proper value for α_C can be found by iterative procedure, as described in the main text.

Experimental Section

The details of the sample fabrication procedure were described elsewhere;[5,28,29] below we will just briefly outline the main steps. The mask for deposition of source-drain electrodes was prepared in advance by E-beam lithography on a silicone chip. The mask has an opening that is about 50 nm wide in the narrowest place, as shown in Figure 2.

The sample chip, together with evaporators for gold and bianthrone, was introduced into a vacuum chamber completely immersed in liquid He. All subsequent fabrication steps, including depositing electrodes and catching the molecule, and the measurements were done without breaking these UHV vacuum conditions. This ensures that electrodes are perfectly clean and there are no contaminations that can be mistaken for the bianthrone molecule.

To prepare a nanogap between two macroscopic electrodes, we first deposited gold at a 45° angle. For such an inclined deposition, the narrowest part of the mask is closed, as illustrated in Figure 2, right, and the deposited gold forms two self-aligned electrodes separated with a gap. To reduce the gap width down to the desired molecular scale of a few nanometers, we decrease the tilt angle by steps of 5°. Each tilt decrease is followed by deposition of approximately 20 Å of gold, which is below the percolation limit. At some critical tilt angle α_C, when the mask is eventually opened, we detect conductivity through a network of gold grains bridging two continuous electrodes. A few more gold depositions at the same angle α_C merge some gold grains together or with electrodes and finally reduce the sample topology to a single gap separating two macroscopic electrodes. At this stage, the gap is typically too narrow, the gap tunneling

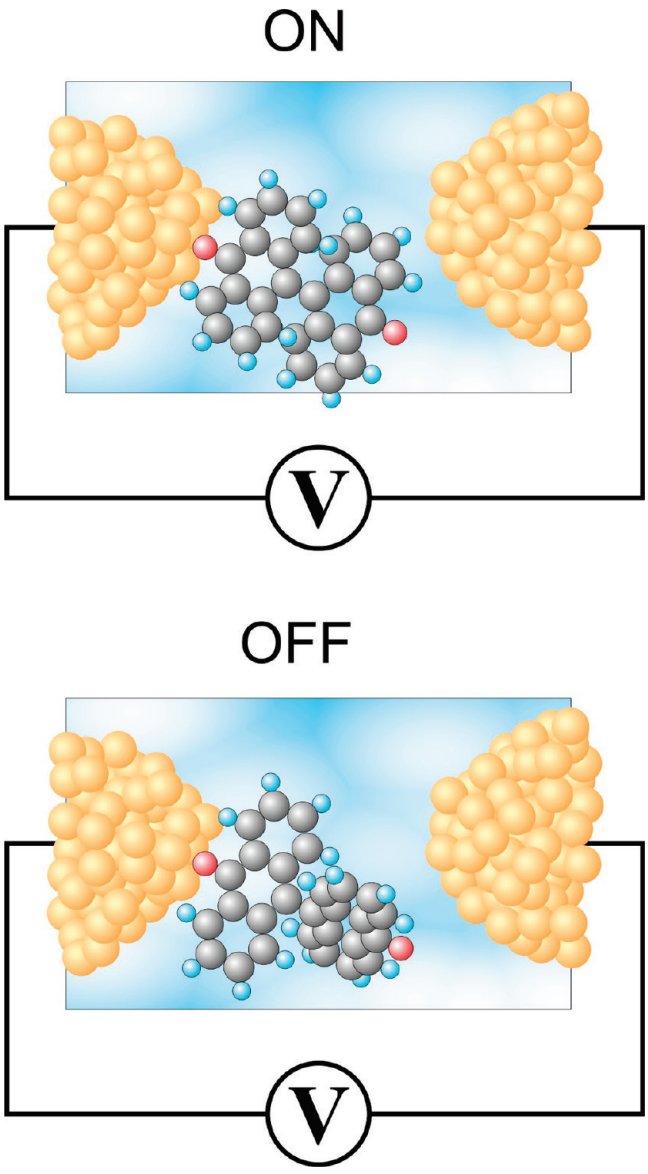

Figure 3. Likely sample geometry and the switching mechanism. The bianthrone molecule is connected to one electrode and separated from the other by a tunneling gap. Switching from the A form to the B form changes the tunneling gap and therefore the resistance of the device.

resistance being in the range of a few megaohms. To slightly open the gap, we gently anneal the sample to approximately 100 K. Such annealing smoothes the electrodes' envelopes and increases the gap resistance to a few gigaohms.

Once the nanogap is prepared, we deposit a submonolayer of molecules. In some rare cases the molecule lands in a nanogap during deposition and the sample conductance, in a single step, rises by a few orders of magnitude. More typically, a submonolayer deposition leaves the nanogap intact. To catch the molecule, we raise the temperature to 30−60 K (when the surface diffusion of molecules is activated) and wait until the first conductance jump.

The resulting sample geometry is sketched in Figure 3. We shall note that it is not ensured by the fabrication procedure that the molecule is equally coupled to the source and drain electrodes. It is, in fact, most likely that the coupling is asymmetric: the molecule is in touch with one electrode and separated from the other by a tunneling gap. This type of topology we observed, for example, for fullerene-based molecular samples.[10,29] The sample resistance for this geometry

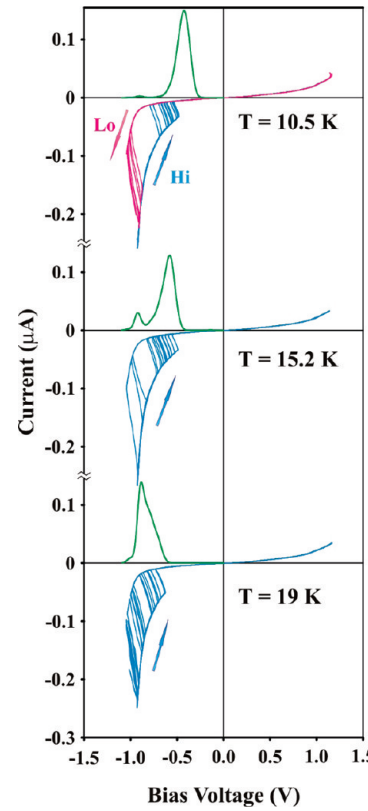

Figure 4. $I-V$ curves traced from negative to positive bias (blue) and in the reverse direction (red), taken at 10.5 K. For higher temperatures, 15.2 and 19 K, only $I-V$ curves taken in the forward direction are shown for clarity (as the areas for forward and reverse switching start to overlap). For each temperature a few hundred $I(V)$ curves were recorded; only 32 representative traces are shown. The green curves show the distribution of switching biases.

depends exclusively on the width of the tunneling gap, which can vary from sample to sample, so that the overall sample conductance for different samples ranges from a few megaohms to 100 MΩ. Any conformational change of the bianthrone molecule should affect the tunneling gap width and therefore the sample resistance; therefore, we expect this molecular device to operate as a purely mechanical switch with the bianthrone kernel as a toggle.

Measurement Results and Analysis

All the samples we measured demonstrated hysteretic switching between two states. The representative data taken for one sample are shown in Figure 4. For the negative to positive bias sweeps the sample is initially in the "Hi" state and will eventually switch to the "Lo" state (we shall call the two states "Hi" and "Lo" according to the value of the current through the molecular junction). For different scans, the switching occurs at slightly different biases, though all switching events are obviously clustered around some characteristic bias. The green plots in Figure 4 present the distribution of switching biases for Hi → Lo switching events. Each switching event observed at the bias voltage V_i is represented as the Gaussian with the width $\delta = 20$ mV and the sum over all switching events $\Sigma\exp[-(V - V_i)^2/\delta^2]$ is shown in Figure 4.

One can clearly see that at higher temperatures the distribution shifts toward negative biases. The fact that the switching is temperature dependent implies that the barrier between two conformations is dramatically reduced as compared to that for BA in solution. We shall first refer to simple qualitative

arguments, following the same lines of reasoning as in refs 10 and 29 more quantitative analysis will then follow.

The switching rate can be estimated as

$$\Gamma \approx \frac{\omega_0}{2\pi} \exp\left[-\frac{U}{\langle E\rangle}\right] \quad (1)$$

where the attempt frequency ω_0 is the characteristic frequency for vibrations along the reaction coordinate, U is the barrier height for Hi → Lo transition and $\langle E\rangle$ is the average vibration energy along the reaction coordinate.

The barrier U depends on the bias voltage, since at positive biases the barrier is suppressed. At extreme negative biases, the barrier is rather high and the Hi state is stable. When the bias is swept in negative-to-positive direction, the barrier height drops and the escape rate Γ increases. As soon as Γ approaches $\sim 1/T_{scan}$ (where $T_{scan} \approx 10$ s is a typical scan time), the molecule switches. At higher temperatures the vibration energy $\langle E\rangle$ is higher and the system can escape earlier at negative biases, where the barrier is higher. That is why the switching area in Figure 4 shifts to the left at $T = 19$ K.

Apart from the temperature, the energy $\langle E\rangle$ has, in principle, two more contributions: the energy supplied by passing electrons and quantum-mechanical fluctuations. The energy supplied by transport current does not depend on temperature (at least not at temperatures as low as 20 K). If the current-induced heating dominates, the average energy $\langle E\rangle$ essentially depends on the transport current only and the temperature makes no substantial effect on switching. As we do observe the temperature effect, we can, in first approximation, assume that the reaction coordinate is at thermal equilibrium with the environment. Then the vibration energy is given by a well-known formula for quantum oscillator coupled to a thermal bath:[30,31]

$$\langle E\rangle = \frac{\hbar\omega_0}{2} \coth\left(\frac{\hbar\omega_0}{2k_B T}\right) \quad (2)$$

For high temperatures ($k_B T \gg \hbar\omega_0$) (2) reduces to $k_B T$ and (1) transforms into a classical Gibbs probability for thermally activated switching. At zero temperatures, $\langle E\rangle = \hbar\omega_0/2$ and the escape rate Γ reduces to the quantum-mechanical tunneling rate through a truncated harmonic potential.[10,32] At low temperatures Γ essentially saturates when the argument of the coth function exceeds 2. It means that one can only see the temperature dependence down to $\tilde{T} = 10$ K if $\hbar\omega_0 < 4k_B\tilde{T} = 3.5$ meV. Solving (1) for U, we can estimate the maximum barrier height as

$$U \approx \frac{\hbar\omega_0}{2} \ln\left(\frac{\omega_0}{2\pi\Gamma}\right) \approx 50\text{meV}$$

To reinforce these qualitative arguments, we shall now turn to a more rigorous analysis of the experimental data.

We consider a general system that starts evolving from some metastable state. The barrier that confines the metastable state is time-dependent and reduces as the time goes. If the transition is characterized by some escape rate $\Gamma(t)$, then the probability $Q(t)$ that at time t the sample is still in the initial state (i.e., that the switching has not happened) is given by a simple rate equation

$$\frac{\mathrm{d}}{\mathrm{d}t} Q(t) = -\Gamma(t)\, Q(t) \quad (3)$$

Since the bias voltage in experiment is incremented with a constant sweep rate $V(t) = V_0 + \dot{u}t$, we can rewrite (3) as

$$\frac{\mathrm{d}}{\mathrm{d}V} Q(V) = -\frac{1}{\dot{u}}\Gamma(V)\, Q(V) \quad (4)$$

This can be easily solved to find the distribution of switching events, which is the probability density $P(V) = (\mathrm{d}/\mathrm{d}V)Q(V)$ that the switching will happen at bias V:

$$P(V) = \frac{\Gamma(V)}{\dot{u}} \exp\left[-\int_{V_0}^{V} \frac{\Gamma(V')}{\dot{u}}\, \mathrm{d}V'\right] \quad (5)$$

Formula 5 gives the distribution of switching events for any given escape rate $\Gamma(V)$. It can be solved for Γ to find the escape rate from the measured distribution of the switching events:

$$\Gamma(V) = \dot{u}\frac{P(V)}{1 - \int_{V_0}^{V} P(V')\, \mathrm{d}V'} \quad (6)$$

We shall stress that (6) is the direct transform of the experimental data for $P(V)$; so far, we made no assumptions about the nature of Hi/Lo states nor about the switching mechanism.

The switching statistics was collected for four different samples; the results are presented in Figure 5.

One can see that the switching rate increases roughly as the exponent of the bias voltage (note the logarithmic scale on the bottom panel). Knowing from eq 1 that $U \sim \log\Gamma$, we conclude that the barrier height is roughly a linear function of the bias voltage:

$$U(V) = U_0 + \alpha V \quad (5)$$

Collecting (1), (2), and (5) together, we have for the tunneling rates

$$\Gamma \approx \frac{\omega_0}{2\pi} \exp\left[-\frac{U_0 + \alpha V}{E_0 \coth(E_0/k_B T)}\right] \quad (6)$$

where $E_0 = {}^1/_2\hbar\omega_0$ is the ground-state energy for vibrations along the reaction coordinate.

The fit based on the (6) is depicted in Figure 5 with dashed lines. The fitting procedure is rather straightforward. First, we choose $\hbar\omega_0 = 3.6$ meV so that the Γ plots for the first sample taken at different temperatures are properly spaced. As discussed earlier, E_0 controls the magnitude of the temperature effect on Γ: if we choose $E_0 \ll k_B T$, the temperature effect will be too strong and the Γ plots for $T = 10.5$ K and $T = 19$ K will be spaced too far away, while in the opposite case, $E_0 \gg k_B T$, there will be no temperature effect at all. We then set the proper α and U_0 for first sample (the parameter α controls the slope and U_0 the vertical offset of the Γ plot). Finally, assuming that ω_0 is essentially the same for all the measured samples,[33] we fit parameters α and U_0 for the other three samples. The parameter α, as extracted from the fit, ranges from 0.03 to 0.1 for different samples. It implies that the bianthrone molecule is charged slightly differently in states "ON" and "OFF", the difference

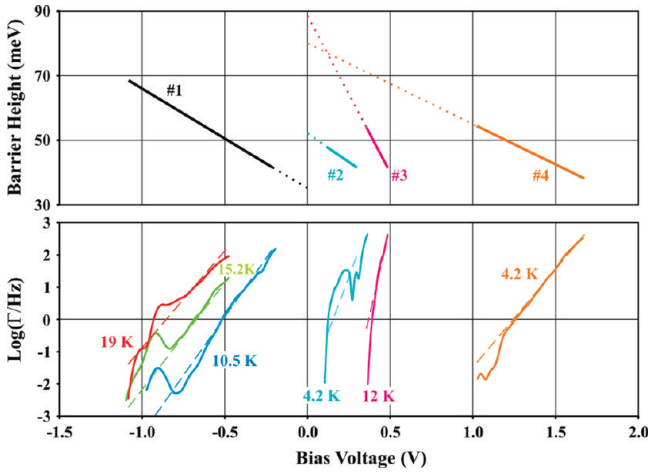

Figure 5. Bottom: switching rates $\Gamma(V)$ for four different samples. For sample #1 the switching statistics was collected at three different temperatures: 10.5, 15.2. and 19 K. The fits based on the formula (6) are depicted with dashed lines. Top: reconstructed barrier height $U(V)$.

being in the range 0.03−0.1 lel. When the molecule switches, some charge goes to/from the electrode and bias-induced electrostatic forces contribute to the total switching energy. In the first approximation, this effect is linear in terms of the bias voltage, as suggested by (5). A sample to sample variation can be attributed to different positioning of the molecule in various samples.

The top panel in Figure 5 presents the reconstructed barrier heights U for all measured samples, as defined by formula (5). The zero-bias barrier height U_0 (which can be extracted from $U(V)$ plots in Figure 5 by linear extrapolation to zero bias) ranges for different samples from 35 to 90 meV.

A more elaborate model, which accounts for possible current-induced contribution to molecular vibrations,

$$\langle E\rangle = \frac{\hbar\omega_0}{2}\coth\left(\frac{\hbar\omega_0}{2k_BT}\right) + \gamma|V| \qquad (7)$$

where γ is a parameter that characterizes electron−phonon coupling (see ref 10 for details), makes the fit only marginally better. For all values of γ consistent with the data in Figure 5 the value of U_0 did not change much.

Of course, by introducing more advanced models (current-induced heating, nonlinear $U(V)$, etc.) and additional fitting parameters, we could make more precise fits. Unfortunately, we do not have enough switching data to justify anything but the simplest possible model. Typically, the sample died after a few thousand switching events: either the nanogap collapsed into metallic contact or the molecule escaped, leaving the nanogap with its original resistance in the range a few gigaohms.[34] We shall stress that, for a molecular switch, the stability at the level of $\sim 10^3$ cycles is extraordinarily high.[35] Only one sample (#1) survived a few thousand switchings at three different temperatures. For sample #2, only 64 switching events were registered, thus explaining why the Γ plot for this sample has excessive noise. A few more samples died before any representative statistics was collected; they are therefore not presented in Figure 5.

Most failures happened when the sample was biased with a maximum voltage; the failure risk rapidly increases for $|V| > 1$ V. For this reason, we do not have representative statistics for switching in the opposite direction. For some traces in positive-to-negative direction, the Lo → Hi switching did not happened before the bias reached the minimum value of −1 V, but instead at some later moment, when the bias sweep was already on the way back from −1 V to zero. An attempt to increase the bias to collect valid statistics destroyed the sample.

Therefore, we lack comprehensive statistics for switching events in the opposite direction. A hint for its barrier is possibly provided by the double-peak shape of the switching histograms for the forward switching: one can clearly see second maxima at bias voltages around 0.9 V in Figure 4. The corresponding plots for escape rates Γ's in Figure 5 also reveal pronounced maxima at the same biases. We can therefore speculate that when the bias approaches 1 V another switching mechanism comes into play, which is also responsible for the reverse switching, with a characteristic barrier on the order of 1 eV.

To summarize, we can reliably infer from our experimental data that the barrier for at least the Hi → Lo transition does not exceed the value of 35−90 meV. Inspired by this experimental evidence for dramatic barrier suppression, we decided to undertake model calculations for the bianthrone molecule placed in a solid-state device.

Quantum-Chemical Modeling

The aim of our quantum-chemical modeling of BA isomerization is to assess the energetic landscape of isomerization, which is the key aspect in its switching behavior. We will describe below the structure and relative stability of various forms of BA and the influence of a metal surface.

We start by summarizing our understanding of the structure and relevant properties of BA in its electronic ground state based on hybrid DFT B3LYP/6-31g** calculations (for methodological details and justification and also for a detailed discussion of molecular geometry, see Supporting Information) to explain what is special about this molecule to make it a realistic candidate for conformational switching.

Both isomers of neutral BA (the structures are shown in Figure 6) correspond well to a quinoid valence structure, with a double bond in the middle and sufficient conjugation between the anthracenes, though the immediate surrounding of the double bond is practically coplanar in A but rather twisted in B. The calculated relative stability of the isomers at the B3LYP level predicts A to be more stable than B by 0.12 eV (Figure 7), in excellent agreement with the experimental value of 3 kcal/mol (0.13 eV).[36,37]

As a quinone, BA is an electron acceptor, so it is relevant to consider its radical anion forms in the context of adsorption on metal and electron transport. Their structures are found to be qualitatively similar to the neutral ones, shown in Figure 6. The principal differences in geometry of the neutral and anionic forms can be understood within a simple orbital picture putting the additional electron to the LUMO of the molecule, which is basically the π^* MO of the central double bond. The relative stability of the anionic forms is predicted to be inverted vs neutral BA: B is calculated to be more stable than A by 0.88 eV (Figure 7), in excellent agreement with the experimental value of 18 kcal/mol (0.78 eV).[36] The most important factor responsible for the reversal of the relative stability of the forms in the anionic BA is certainly the difference in the vertical electron affinities of the forms (Figure 7), which increases with the twist angle between the antraquinones in BA, in perfect correlation with the decreasing LUMO energy; see the Supporting Information for more details.

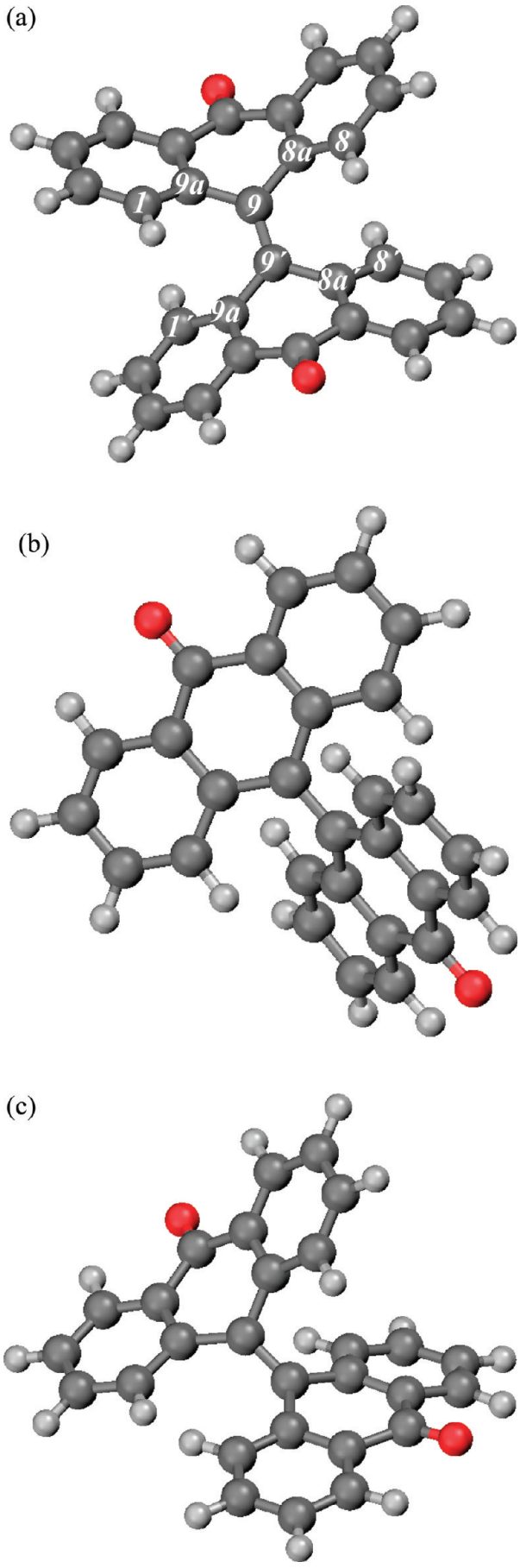

Figure 6. Structures of bianthrone optimized at the B3LYP/6-31g** level: (a) neutral form A with conventional atom numbering; (b) neutral form B; (c) neutral transition state.

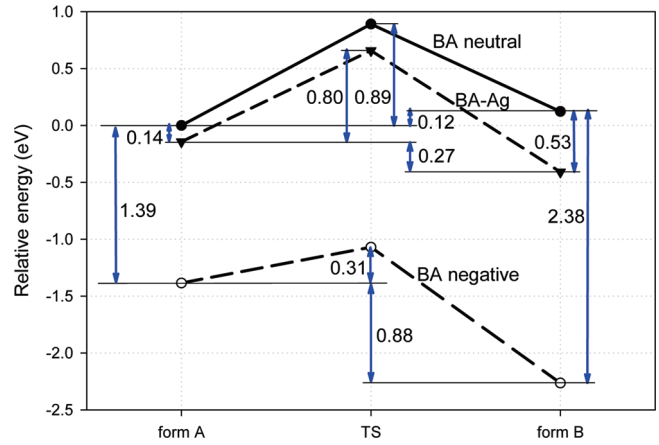

Figure 7. Calculated relative energies for the essential structures of free bianthrone and its complex with Ag.

While the structures of the neutral and charged isomers have already been studied theoretically, the transition states (TS) of BA have not been identified, to the best of our knowledge. Characterizing them is of crucial importance for the assessment of BA interconversion and of the influence of the surface in this process, so we have obtained the structures for the TS (characterized by the only imaginary frequency corresponding to the reaction coordinate) of neutral BA, whose structure is shown in Figure 6c, and also of the BA radical ion, which is quite similar; both discussed in more detail in the Supporting Information.

The neutral TS is 0.89 eV higher than the stable A form (Figure 7), in excellent agreement with the experimental value of 0.87 eV.[36−38] This is a low value, compared to those typical for rotations around a double bond, which is due to the ground-state destabilization, rather than to some particular stabilization of the TS. A low isomerization barrier makes BA thermochromic in solution, in other words, switchable at room temperature. However, this barrier is still high compared to the value estimated for low-temperature switching in the junction.

For the radical anion, the A to B isomerization barrier is further decreased with respect to the neutral molecule; the calculated value is only 0.31 eV, to be compared with the experimental value of 10.8 kcal/mol (0.47 eV).[24] This lowering of the barrier is again due to increased electron affinity of BA with tilt angle, as well as the reversed stability of the isomers discussed above.

At this stage, it is reasonable to check whether negative charging can be induced by the interaction of BA with metal (silver in particular, as this is the contact material) when the molecule is captured in the junction in our experiments.

We obtained fully optimized structures (Figure 8) for the complexes of Ag with the A and B forms, as well as the transition state for the rearrangement between A and B forms when bound to Ag. The interaction is clearly driven by Ag donation into the vacant orbital including oxygen π-AO. Though the binding geometries for the complexes with the A and B forms are qualitatively similar, the bond strength and charge transfer differ significantly. Silver donates only 0.035 |e| to the A form, and its geometry remains practically the same as in the free molecule. With the B form, 0.353 |e| are donated, leading to more pronounced changes in the geometry of the organic part. The binding energy to A is 0.14 eV, and to B is 0.53 eV (not corrected for the possible basis set superposition error, BSSE), shown in Figure 7. A strong covalent bond with Ag is thus formed only with the B form, with appreciable

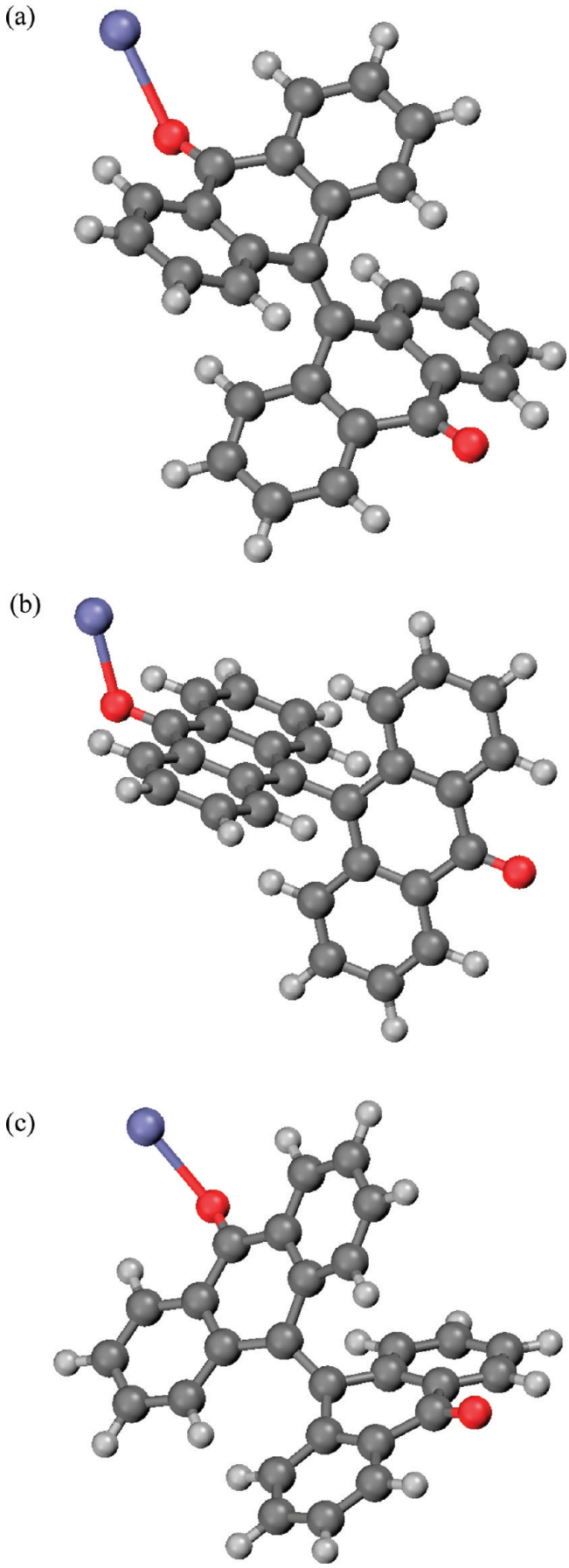

Figure 8. Structures of the bianthrone−Ag complex as optimized at the B3LYP/LANLDZDP level: (a) form A; (b) form B; (c) transition state.

electron transfer to the BA LUMO, leading to a complete loss of the double-bond character of the middle CC bond. Note also that the difference in the binding energies also results in the reversal of the relative stability of the A and B forms upon complexation with Ag. This effect is similar to the negative charging effect but is attained at a much lower charge transferred by virtue of chemical bonding.

The transition-state structure in the complex of BA with Ag is most similar to that of BA alone discussed above (cf. Figures 8c and 6c), as far as the organic part is concerned, and intermediate between Ag−A and Ag−B in their bonding to Ag, and the charge transfer is 0.146 e. The barrier height with respect to Ag−A is 0.80 eV, somewhat lower than for neutral BA without Ag (0.89 eV).

We conclude that specific binding BA to the Ag electrode exerts profound influence on the relative stability of its forms and is likely to influence the equilibrium between them. Note that the Fermi level (workfunction) of metals, equal to their electron affinity and ionization potential, is lying in the HOMO−LUMO gap of the corresponding metal atom, which makes bulk metal surfaces more easily ionizable than the atoms of the same element. We have all grounds to expect, therefore, that negative charges in all BA forms contacting silver in the junction are proportionally higher than those discussed above for their Ag−BA complexes.

As BA is charged, it is relevant to consider the possible role of the image charge effects. Here, we wonder, in particular, if the barrier for the interconversion can be lowered either by geometric distortion induced when the molecule is pressed onto the surface by the image attractive force, or by different stabilization energy of the forms even in the absence of significant geometric distortions. We will model the image interaction of the BA forms bearing the negative charge of full −|e| and the neutral forms (whose atoms are still effectively charged due to internal polarization inherent to any heteroatomic molecule) in order to determine the limits for the partially charged species.

The effect of a polarizable bulk (metal or metal oxide, in this case) on a polar or charged molecule can be approximated by the interaction of this molecule with its image charges. The classical image charge model was shown to be fully compatible with DFT; the image plane position is ca. 1 Å away from the outer nuclear plane of the metal.[39] Therefore, the atom−atom contacts at the interface should be considered ca. 1 Å longer than the distances from the atoms in the molecule to the image plane.

We take the Mulliken charges obtained from a calculation on a free molecule as an initial guess for the image charges. The molecule is positioned with respect to the coordinate axes in such a way that the XY plane is the image plane ("metal surface") (Figure 9).

The geometry optimization is carried out under constraints not to let the molecule approach too close the *XY* plane. The image charge values and positions, as well as constraints, are adjusted in the course of optimization if necessary, to reach self-consistence. This image charge model is expected to provide an idea for the interaction energies and geometries at the interface rather than their exact values. The image interaction energy can be defined and obtained from the calculations as the difference between the total energy in the presence of point charges and the sum of the total energy of the free molecule and Coulomb interaction of these point charges between themselves. Note that the image Coulomb interaction energy obtained this way is in perfect agreement with that calculated

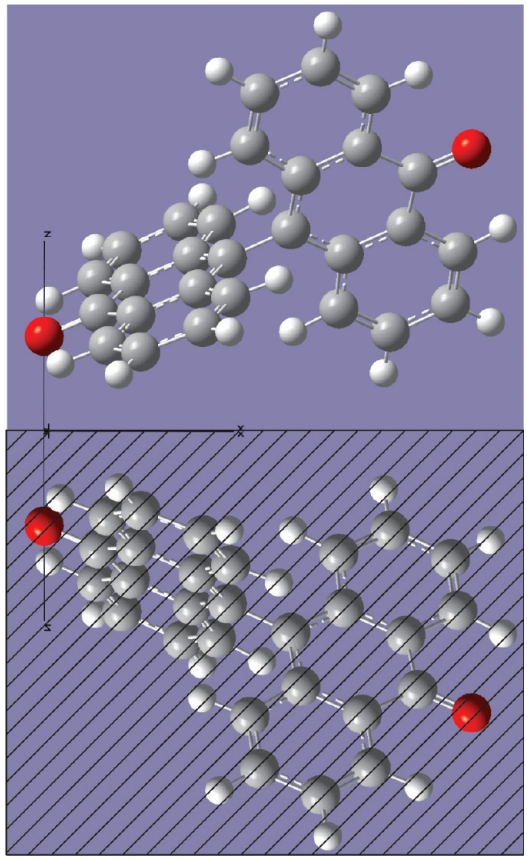

Figure 9. Example of bianthrone arrangement vs its image plane (*x*O*y*).

from a simple classical point charge model between the Mulliken charges of the atoms in the molecule and their images.

For the neutral forms A and B, the initial geometries are those of the free molecules, and their positions vs the image plane are inspired by chemisorbed geometries: one oxygen at *Z* ca. 2 Å, with the corresponding ring forming an angle of 120° with the *Z* axis; the nearest hydrogen distances from the plane are imposed to be no shorter than 1 Å. The calculations indicate that the image interaction energy at this geometry is −0.095 and −0.087 eV for the forms A and B, respectively. Consequently, the driving force of attraction is insufficient to change sensibly the molecular geometry. Moreover, under certain constraints, the image effect makes the molecule turn away from the surface, resembling effective repulsion. Qualitatively, it arises from the specifics of charge distribution in BA; in more detail, this counterintuitive behavior is explained in the Supporting Information. We conclude that the image charge interaction with both conformations of neutral BA is very weak.

For the negative ions, the situation is quite different, though the charge distribution over the molecule does not change qualitatively. However, the net charge on the molecule makes its interaction with the image much stronger and clearly stabilizing, suggesting that the anions would stick to the surface even in the absence of specific chemisorption. Reoptimization of the geometry in the presence of image charges, starting from the arrangement allowing for a close contact of at least one oxygen to the image plane (under the constraints not to let any atom approach the image surface closer than a threshold value of 1 Å) yields the structures shown in Figure 10. While the geometry of the B form is not changed appreciably, one of the anthracene units in the A form undergoes notable planarization, which, in particular, permits its oxygen to decrease the distance

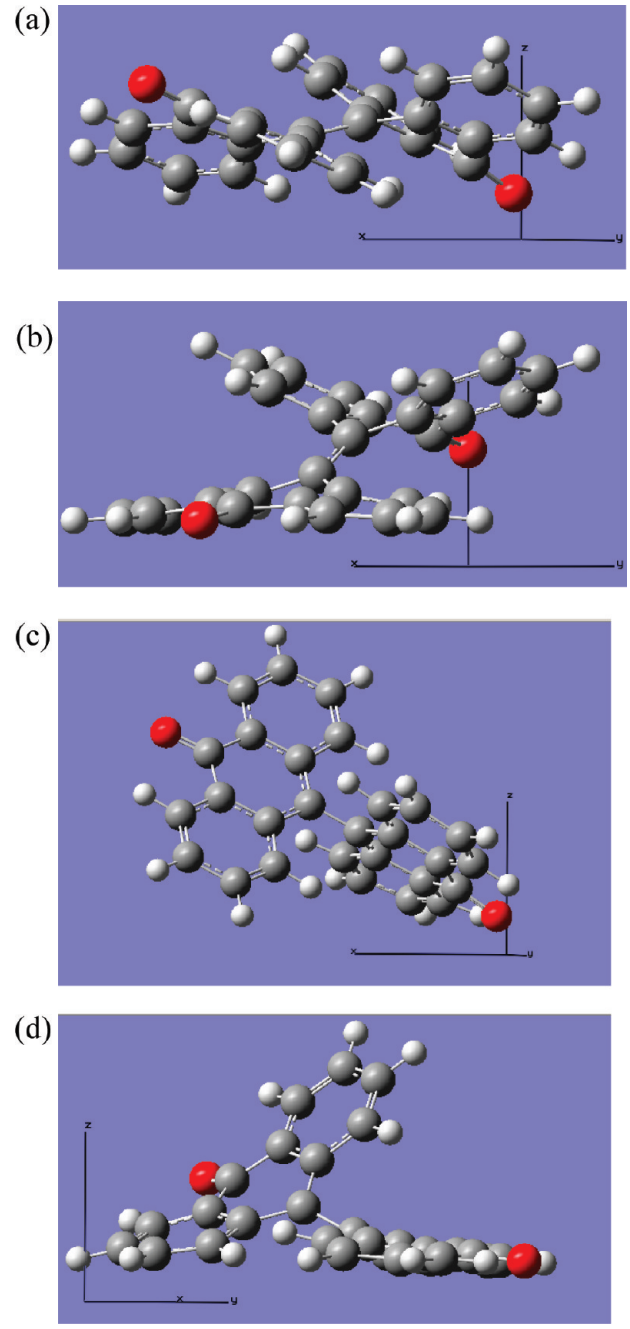

Figure 10. Essential structures of bianthrone radical anion as optimized with B3LYP/6-31g** in the presence of its image charges: (a) form A, higher energy arrangement; (b) form A, lower energy arrangement; (c) form B; (d) transition state.

to its image. As a result, image interaction with the optimized structures is more favorable for A: with respect to the free radical anion, its energy is stabilized by 3.51 eV upon relaxation due to the image effects, compared to 3.21 eV for B. The net relative stabilization of A is thus 0.30 eV. This behavior is robust when the distance from the image plane is tuned: shifting the molecule by 0.5 Å away from the image plane (that is increasing to 3 Å the shortest separation between the atoms and their images) and adjusting the image charge values (without geometry reoptimization), the gain in energy due to image interaction is reduced to 2.40 and 2.18 eV for the A and B forms, respectively, though there remained net relative stabilization by 0.22 eV for A vs B.

This relative stabilization is even more pronounced for the TS taken in its initial geometry and optimized in the presence

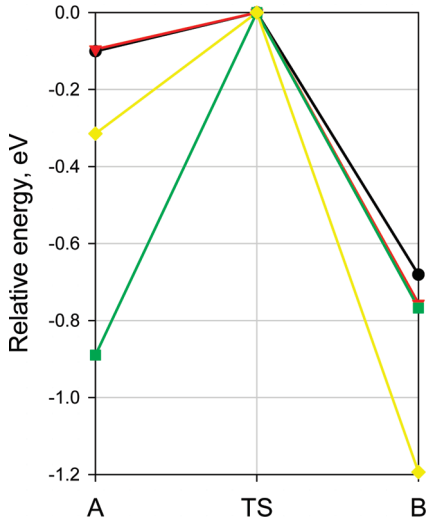

Figure 11. Barrier heights (calculated energies relative to the transition state) for bianthrone: free neutral (green), free radical anion (yellow), and radical anion in the presence of its image charges at minimum distances of 2 Å (black) and 3 Å (red).

of image charges, under the same constraints as above. Similarly to the A form at the surface, TS shows the closest anthracene unit getting planarized. This allows the oxygen of this ring, as well the other oxygen to get closer to their image charges. As a result, the stabilization vs the free radical anion TS attains 3.72 eV at 1 Å and 2.62 eV at 1.5 Å constraint distance from the image plane. This leads to an effective decrease of the barrier for the A anion isomerization to 101 or 97 meV (for 1 and 1.5 Å constraint distance, respectively) (see Figure 11), which is of the order of magnitude suggested by the switching experiments.[40] We stress that the barrier height in the presence of the image charges has rather an indicative value, also due to the fact that both the relative energy of the BA structures and the image interaction energy crucially depends on the actual charge transfer at the interface. Nevertheless, on the basis of these estimates, we are in a position to suggest the following structural mechanism for switching.

The stable bianthrone isomer landing on the surface from the gas phase is the folded form A. In contact with the silver electrode and under bias, it acquires negative charge: this is the initial "Hi" state. Due to the image charge attraction, the isomerization barrier of the anionic form A to B is significantly lowered to the values compatible with those estimated experimentally for Hi → Lo transition (Figure 11). However, the barrier for the isomerization back remains high and less sensitive to the charge state of the molecule. As a result, the backward switching could not be promoted by thermal fluctuations and is likely mediated by some current-induced high-energy excitation.

Conclusion

Conductance measurements on bianthrone in single-molecule junctions revealed conductance bistability and hysteretic switching between high and low conductance states for all samples prepared. The characteristic bias for high-low conductance transition was found to be temperature dependent at temperatures down to 10 K. This observation allows for an estimate of the switching barrier to be below ~100 meV. A more rigorous analysis, based on the statistics of the switching events, allows us to quantify the switching barrier and its bias dependence. For all four samples, which survived enough on−off switchings to collect comprehensive statistics, the barrier height was found to be in the range 35−90 meV; all four samples demonstrated a similar dependence of the barrier height vs the bias voltage. This similarity strongly suggests that the switching mechanism is linked to intrinsic molecular properties, rather than fortuitous junction contact geometry effects. As a matter of fact, bianthrone exists in the form of two stable isomers. However, the experimentally established isomerization barrier for neutral bianthrone in solution (ca. 0.9 eV) is an order of magnitude higher than the values suggested by our analysis for a molecular switch.

To address this apparent contradiction, we carried out detailed quantum-chemical calculations for bianthrone molecules both isolated and simulating solid-state environments. For the neutral single molecule, our computational results are fully consistent with the experimentally established numbers. However, we have found that the isomerization of radical anion proceeds through a lower barrier (ca. 0.3 eV), as also indicated by previous measurements in solution. When placed in contact with silver, one of the bianthrone isomers acquires negative charge that shifts molecular geometry toward the one of the anions, thus lowering the transition barrier. More pronounced barrier suppression arises if one takes into account the interaction between the charge on the molecule and the image charges on the substrate. It appears that the transition state is less rigid than any of the conformations, which allows the atomic charges in the anion to approach closer their images, so that the electrostatic interaction compensates the distortion energy, thus lowering the transition barrier for the anion at a metal surface down to ca. 0.1 eV, in good agreement with our experimental findings.

This result shows that the environment plays a very important role in the performance of single molecules devices; highly polarizable substrates and metallic electrodes can dramatically affect the energy landscape of the molecular kernel. Even if, like in conformational switches, the existence of two states is encoded in molecular design, the crucial operational parameters, switching voltages and the mere existence of bistability, are environmentally sensitive. For the adequate modeling of single-molecule electronic devices the proper treatment of the environment is mandatory.

Acknowledgment. The research leading to these results has received funding from the European Community's Seventh Framework Programme (FP7/2007-2013) under the grant agreement SINGLE no. 213609 and from the Interuniversity Attraction Pole IAP 6/27 Program of the Belgian Federal Government. J.C. is an FNRS research fellow.

Supporting Information Available: Description of our computational methodology, the detailed discussion of the electronic structure and properties of bianthrone isomers and their complexes with Ag, Cartesian coordinates of the optimized structures, and a model explaining a counterintuitive manifestation of the image charge effect. This material is available free of charge via the Internet at http://pubs.acs.org.

References and Notes

(1) Joachim, C.; Ratner, M. A. *Proc. Natl. Acad. Sci. U.S.A.* **2005**, *102*, 8801.
(2) Park, H.; Park, J.; Lim, A. K. L.; Anderson, E. H.; Alivisatos, A. P.; McEuen, P. L. *Nature* **2000**, *407*, 57.
(3) Reed, M. A.; Zhou, C.; Muller, C. J.; Burgin, T. P.; Tour, J. M. *Science* **1997**, *278*, 252.
(4) Kubatkin, S.; Danilov, A.; Hjort, M.; Cornil, J.; Brédas, J.-L.; Stuhr-Hansen, N.; Hedegård, P.; Bjørnholm, T. *Nature* **2003**, *425*, 698.
(5) Kubatkin, S.; Danilov, A.; Hjort, M.; Cornil, J.; Brédas, J.-L.; Stuhr-Hansen, N.; Hedegård, P.; Bjørnholm, T. *Curr. Appl. Phys.* **2004**, *4*, 554.
(6) Lörtscher, E.; Ciszek, J. W.; Tour, J.; Riel, H. *Small* **2006**, *2*, 973.

(7) Pan, S.; Fu, Q.; Huang, T.; Zhao, A.; Wang, B.; Luo, Y.; Yang, J.; Hou, J. *Proc. Natl. Acad. Sci. U.S.A.* **2009**, *106*, 15259.

(8) He, J.; Chen, F.; Liddell, P. A.; Andreasson, J.; Straight, S. D.; Gust, D.; Moore, T. A.; Moore, A. L.; Li, J.; Sankey, O. F.; Lindsay, S. M. *Nanotechnology* **2005**, *16*, 695.

(9) Fleming, C.; Long, D.-L.; McMillan, N.; Johnston, J.; Bovet, N.; Dhanak, V.; Gadegaard, N.; Kögerler, P.; Cronin, L.; Kadodwala, M. *Nat. Nanotechnol.* **2008**, *3*, 229.

(10) Danilov, A. V.; Hedegård, P.; Golubev, D. S.; Bjørnholm, T.; Kubatkin, S. E. *Nano Lett.* **2008**, *8*, 2393.

(11) Choi, B.-Y.; Kahng, S.-J.; Kim, S.; Kim, H.; Kim, H. W.; Song, Y. J.; Ihm, J.; Kuk, Y. *Phys. Rev. Lett.* **2006**, *96*, 156106.

(12) Kumar, A. S.; Ye, T.; Takami, T.; Yu, B.-C.; Flatt, A. K.; Tour, J. M.; Weiss, P. S. *Nano Lett.* **2008**, *8*, 1644.

(13) Donhauser, Z. J.; Mantooth, B. A.; Kelly, K. F.; Bumm, L. A.; Monnell, J. D.; Stapleton, J. J.; Price, D. W., Jr.; Rawlett, A. M.; Allara, D. L.; Tour, J. M.; Weiss, P. S. *Science* **2001**, *292*, 2303.

(14) Loppacher, Ch.; Guggisberg, M.; Pfeiffer, O.; Meyer, E.; Bammerlin, M.; Lüthi, R.; Schlittler, R.; Gimzewski, J. K.; Tang, H.; Joachim, C. *Phys. Rev. Lett.* **2003**, *90*, 066107.

(15) Luo, Y.; Collier, C. P.; Jeppesen, J. O.; Nielsen, K. A.; DeIonno, E.; Ho, G.; Perkins, J.; Tseng, H.-R.; Yamamoto, T.; Stoddart, J. F.; Heath, J. R. *ChemPhysChem* **2002**, *3*, 519.

(16) Collier, C. P.; Mattersteig, G.; Wong, E. W.; Luo, Y.; Beverly, K.; Sampaio, J.; Raymo, F. M.; Stoddart, J. F.; Heath, J. R. *Science* **2000**, *289*, 1172.

(17) Kaasbjerg, K.; Flensberg, K. *Nano Lett.* **2008**, *8*, 3809.

(18) Thygesen, K. S.; Rubio, A. *Phys. Rev. Lett.* **2009**, *102*, 046802.

(19) Korenstein, R.; Muszkat, K. A.; Sharafy-Ozeri, S. *J. Am. Chem. Soc.* **1973**, *95*, 6177.

(20) Biedermann, P. U.; Stezowski, J. J.; Agranat, I. *Eur. J. Org. Chem.* **2001**, 15.

(21) Biedermann, P. U.; Stezowski, J. J.; Agranat, I. Overcrowded Polyciclic Aromatic Enes. *Advances in Theoretically interesting molecules*; JAI Press: 1998; Vol. 4, pp 245−322.

(22) Kikuchi, O.; Kawakami, Y. *J. Mol. Struct. THEOCHEM* **1986**, *137*, 365.

(23) Olsen, B. A.; Evans, D. H. *J. Am. Chem. Soc.* **1981**, *103*, 839.

(24) Neta, P.; Evans, D. H. *J. Am. Chem. Soc.* **1981**, *103*, 7041.

(25) Jørgensen, M.; Lerstrup, K.; Frederiksen, P.; Bjørnholm, T.; Sommer-Larsen, P.; Schaumburg, K.; Brunfeldt, K.; Bechgaard, K. *J. Org. Chem.* **1993**, *58*, 2785.

(26) Sommer-Larsen, P.; Bjørnholm, T.; Jørgensen, M.; Lerstrup, K.; Frederiksen, P.; Schaumburg, K.; Brunfeldt, K.; Bechgaard, K.; Roth, S.; Poplawski, J.; Byrne, H.; Anders, J.; Eriksson, L.; Wilbrandt, R.; Frederiksen, J. *Mol. Cryst. Liq. Cryst.* **1993**, *234*, 89.

(27) Cuberes, M. T.; Schlittler, R. R.; Jung, T. A.; Schaumburg, K.; Gimzewski, J. K. *Surf. Sci.* **1997**, *383*, 37.

(28) Kubatkin, S. E.; Danilov, A. V.; Olin, H.; Claeson, T. *J. Low Temp. Phys.* **2000**, *118*, 307.

(29) Danilov, A. V.; Kubatkin, S. E.; Kafanov, S. G.; Bjørnholm, T. *Faraday Discuss.* **2006**, *131*, 337.

(30) Feynman, R. *Frontiers in Physics, Statistical Mechanics*; Adison-Wesley Publishing Co.: New York, NY, U.S., 1972; p 53.

(31) Brandbyge, M.; Hedegård, P. *Phys. Rev. Lett.* **1994**, *72*, 2919.

(32) For an arbitrary shape of potential barrier the tunneling rate depends both on the barrier height and on the barrier width. But for a truncated harmonic potential the height and the width are related so that the tunneling rate depends on a single parameter, ω_0.

(33) Here we assume (and the calculations presented below justify this assumption) that the molecular distortion due to interation with surface and/or bias-induced elecric field is moderate, so that the frequencies of intramolecular vibrations are not disturbed much.

(34) The switches based on a simple C_{60} molecule were much more robust and survived more than 10^5 On-Off switchings, see refs 10 and 29.

(35) Compare to MTBF $\sim 10^4$ (mean time between failures) for standard non-volatile CMOS switch.

(36) Agranat, I.; Tapuhi, Y. *J. Org. Chem.* **1979**, *44*, 1941.

(37) Agranat, I.; Kalisky, O.; Tapuhi, Y. *J. Org. Chem.* **1979**, *44*, 1949.

(38) Agranat, I.; Tapuhi, Y. *J. Am. Chem. Soc.* **1976**, *98*, 615.

(39) Lang, N. D.; Kohn, W. *Phys. Rev. B* **1973**, *7*, 3541.

(40) It should be noted that the structure obtained as a result of this optimization cannot be rigorously called the transition state. Indeed, TS identification normally requires fully unrestricted geometry optimization and vibrational mode check, which is not feasible in our model with the constraints imposed. Still, there all grounds to believe that the structure discussed is close to the true TS at the surface, as molecular rearrangement at the surface anyway logically has to follow a pathway similar to that of the free molecule. Note also that this TS-like structure is indeed stabilized by the presence of the image charges as the molecule is pressed to the surface by attraction: with the image charges removed, still in the presence of surface constraints, the structure unfolds to one of the isomers (B for the anion, A for the neutral).

JP1060667